Taylor & Francis
Taylor & Francis Group

Combustion Theory and Modelling

ISSN: (Print) (Online) Journal homepage: https://www.tandfonline.com/loi/tctm20

Response of one-dimensional ionised layer to oscillatory electric fields

Narjisse Kabbaj & Hong G. Im

To cite this article: Narjisse Kabbaj & Hong G. Im (2023) Response of one-dimensional ionised layer to oscillatory electric fields, Combustion Theory and Modelling, 27:2, 267-289, DOI: 10.1080/13647830.2023.2165965

To link to this article: https://doi.org/10.1080/13647830.2023.2165965

Combustion Theory and Modelling, 2023
Vol. 27, No. 2, 267–289, https://doi.org/10.1080/13647830.2023.2165965

Response of one-dimensional ionised layer to oscillatory electric fields

Narjisse Kabbaj[a,b] and Hong G. Im [a*]

[a]*Clean Combustion Research Center, King Abdullah University of Science and Technology, Thuwal, Saudi Arabia;* [b]*Department of Electrical and Computer Engineering, College of Engineering, Effat University, Jeddah, Saudi Arabia*

(*Received 16 February 2021; accepted 11 December 2022*)

To provide fundamental insights into the response of laminar flames to alternating current (AC) electric fields, a simplified one-dimensional model using an ionised layer model is formulated with the conservation equations for the ion species with ionisation, recombination, and transport due to molecular diffusion and electric mobility. A parametric study is conducted to investigate the response of the ion layer at different voltages and oscillation frequencies, and the results are examined mainly in terms of the net current–voltage (I–V) characteristics. As the oscillation frequency is increased, a nonmonotonic response in the I–V curve is seen such that the current may exceed the saturation condition corresponding to the steady DC condition. In general the current reaches a peak as the unsteady time scale becomes comparable to the ion transport time scale, which is dictated by the mobility, and eventually becomes attenuated at higher frequencies to behave like a low-pass filter. The extent of the peak current rise and the cut-off frequency are found to depend on the characteristic time scales of the ion chemistry and mobility-induced transport. The simplified model serves as a framework to characterise the behaviour of complex flames in terms of the dominant ionisation and transport processes. The current overshoot behaviour may also imply that the overall effect of the electric field may be further magnified under the AC conditions, motivating further studies of multi-dimensional flames for the ionic wind effects.

Keywords: electric field effects; ion transport; unsteady flames; AC voltage response

1. Introduction

All flames produce weakly ionised plasmas. As such, modifying flame characteristics by applying an external electric field has been studied for many decades, with potential benefits including reduced soot emission [1–5], enhanced flame propagation [6–10], and augmented flame stability [11–14]. While the exact mechanism by which the electric field influence the flame behaviour is a subject of continuing study, one of the most plausible explanations, at the voltage level up to a few kV, is the electro-hydrodynamic effect, also known as the ionic wind effect [15–20], which refers to the generation of a body force due to the collision of ions with the surrounding neutral molecules, altering the convective bulk flow field. Charged molecules such as positive and negative ions and electrons are generated in a flame zone through chemi-ionisation [21–27] and subsequent ion chemistry. Diffusion of the charged molecules is also affected by the Lorentz force in the form of mobility. The effect of applied voltage on the motion of the electrons and ions is commonly

*Corresponding author. Email: hong.im@kaust.edu.sa

This article has been corrected with minor changes. These changes do not impact the academic content of the article.

characterised by the induced current versus voltage, namely the I–V curve. Since the rate of ion generation is limited by the flame chemistry, the current typically increases with the applied voltage in the 'sub-saturated' conditions and levels off as the voltage reaches the 'saturated' condition, beyond which an increased voltage no longer produces additional charged species [16,28,29].

The study of the ionic wind effects dates back to the 1960s [15] and a summary of the early work can be found [23]. For fundamental characterisation, two configurations have frequently been adopted: two-electrode and single-electrode circuits. In the former [18,30], an electrode is placed horizontally near or in the flame and a second electrode is positioned at the injector level. This positioning leads to higher currents, but it may cause problems such as geometrical limitation and contamination of the electrode placed in the flame because of its exposure to hot burned gases. In this regard, a single-electrode configuration (without a ground electrode), in which the metallic injector nozzle serves as a high-voltage electrode, was also proposed [1]. This configuration has been used to study the effects of electric fields on the stabilisation characteristics of propane-lifted flames in turbulent [31] and laminar jets [32]. The effect was found minimal when applying direct current (DC) voltages, while Won et al. [32] reported that the ionic wind effects become significant by applying alternating current (AC) voltages at lower frequencies.

Flame characteristics in response to AC voltages are of practical interest but have not been studied extensively due to the complex nature of the physical problem. Since combustion involves various physical and chemical processes with a broad range of length and time scales, it is expected that unsteady oscillations of the electric field may reveal flame behaviour that is substantially different from a straightforward extension of the findings from previous studies with the DC electric field. For example, with high-frequency AC electric fields at 1–10 MHz [8] and a microwave range [33], electrons are accelerated while ions remain nearly immobile so that the energy coupling is only made in the form of electron heating, which in turn promotes vibrational excitation of the mixture. At lower frequencies, the energy is coupled to the ions with larger mass, thus introducing an ion-driven wind [15] that modifies the flow field around the flame.

Recently, Park et al. [34] conducted an experimental study of non-premixed flames in a counterflow configuration by applying AC electric fields at different frequencies between the two nozzles. They reported that the flame response is divided into two regimes: (a) a plateau of flame oscillation amplitude at lower frequencies ($< \sim 20$Hz), which seems to be controlled by geometrical parameters governing the transport process, and (b) a decaying flame amplitude at higher frequencies, exhibiting a scaling with the Stokes parameter, defined as the ratio of the unsteady frequency to the global strain rate. An important finding in this study was the occurrence of the 'double stagnation planes' at higher voltage beyond the saturation condition, which is explained as the result of bidirectional ionic winds, i.e. positive and negative ions moving in the opposite direction when the applied AC field is properly 'phase-locked'. In contrast, Guerra-Garcia et al. [35] reported resonance behaviour in the oscillation amplitude of the flame at different, but no corresponding I–V response was reported for quantitative validation of computational predictions. Escalpez et al. [36] computationally studied the behaviour of the burner-stabilised premixed flame subjected to AC conditions. They found that for higher frequencies, the electrons are close to equilibrium, but the slower ions do not reach the steady state, changing the current drawn from the flame and possibly inducing an asymmetric ionic wind due to the diodic effect; and for very high frequencies the ions are too slow to respond to the change in external electric potential and the ionic wind. Due to the complex nature of the underlying physics and

ion chemistry, physical explanations of observed experimental phenomena remain controversial, and ultimately high fidelity multi-dimensional computational simulations are needed. In the meantime, it is sensible to start with a simplified model to isolate several key mechanisms, such as ion-electron chemistry, ion-electron diffusion-mobility, and ionic wind effect. The present study is a first attempt to focus on the interaction between chemistry and mobility, in a simplified one-dimensional geometry to allow extensive parametric studies.

While the idealised 1D configuration is inadequate for reproducing realistic ionic wind effects which are inherently multi-dimensional, the main premise of the present study is to identify different chemical and transport time scales of a large number of charged species and the corresponding flame characteristics as the AC voltage and frequency are varied. The present model eliminates complex flow-chemistry interactions and isolates the electric field effects on the motion of positive and negative ions in 1D space, thus providing clear insights into the basic coupling between the ion transport and the electric field. The results of the present study are a vehicle to investigate more complex flame behaviour and will serve as a building block towards realistic multi-dimensional simulations to reproduce and explain the experimental observations. In our future work, additional realisms such as multi-dimensionality and detailed chemistry will be added to attempt direct comparisons with experimental results.

2. Formulation and physical consideration

The adopted 1D model configuration is shown in Figure 1. An electrode with a specified time-varying voltage and a ground electrode are separated by a distance L. A model flame is represented by an ionisation layer with a Gaussian profile, located in the centre of the domain. Positive and negative ions are generated inside the ionisation layer at a given finite rate and are subsequently transported to either side of the electrodes by both molecular diffusion and drift diffusion in response to the applied electric field.

Note that the 1D model is unable to describe the associated flow field in a realistic way, so that the convective flow and momentum transfer between the charged species to the background neutrals is neglected. This implies that the ionic wind effects are excluded from the present study. The main objective is to conduct a parametric study to understand the basic behaviour of flame-generated ions, such as their spatial distribution and the resulting

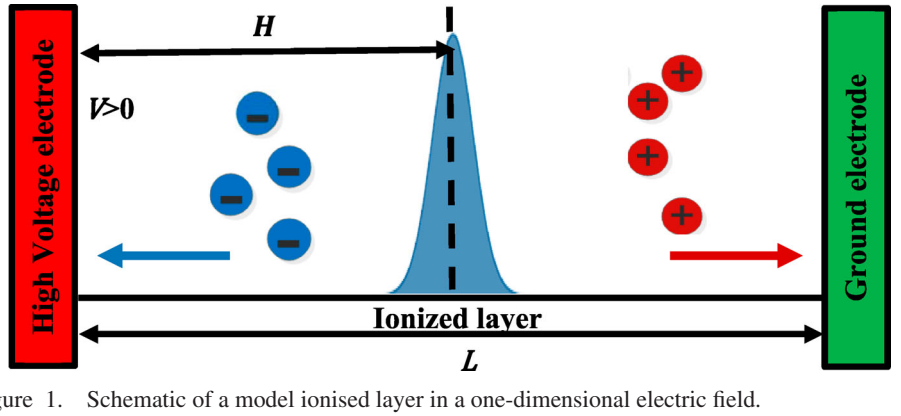

Figure 1. Schematic of a model ionised layer in a one-dimensional electric field.

I–V characteristics, in response to the imposed electric field. Following the previous studies [19,37], the 1D transport equations for positive and negative ions are written as:

$$\frac{\partial n_+}{\partial t} + \frac{\partial}{\partial x}\left[-D_+\frac{\partial n_+}{\partial x} - K_+ n_+ \frac{\partial V}{\partial x}\right] = k_i g - k_r n_+ n_- \tag{1}$$

$$\frac{\partial n_-}{\partial t} + \frac{\partial}{\partial x}\left[-D_-\frac{\partial n_-}{\partial x} + K_- n_- \frac{\partial V}{\partial x}\right] = k_i g - k_r n_- n_+ \tag{2}$$

where t is the time, x is the spatial variable, n is the number density of charged species, K is the mobility, D is the molecular diffusivity, k_i and k_r are the ionisation and recombination rate constants, respectively. Subscripts $+$ and $-$ denote the positive and negative ions, respectively. The spatial distribution of the electric potential, V, is determined by the Poisson equation:

$$\frac{\partial^2 V}{\partial x^2} = -\frac{q_e}{\varepsilon}(n_+ - n_-) \tag{3}$$

where q_e is the unit charge (1.6×10^{-19} C) and ε is the vacuum permittivity (8.854×10^{-12} C/V m). Since the energy equation is not directly solved, the ionisation rate is given in the form of a representative a constant Gaussian profile centred at $x = H$ with a thickness a, written as:

$$g = \exp\left[-\frac{\pi (x-H)^2}{a^2}\right] \tag{4}$$

which implies a steady generation of ions in the flame. As for the recombination reaction, in the absence of neutral species, the only possible recombination reaction is between the positive and negative ions.

Equations (1)–(3) are subjected to the following boundary conditions:

$$\begin{aligned}
&V(0,t) = V_{\max}\sin(\omega t) = V_{\max}\sin(2\pi f t); V(L,t) = 0;\\
&V(0,t) < 0 \Rightarrow \frac{\partial n_+(0,t)}{\partial x} = 0; n_-(0,t) = 0; \frac{\partial n_-(L,t)}{\partial x} = 0; n_+(L,t) = 0;\\
&V(0,t) > 0 \Rightarrow \frac{\partial n_-(0,t)}{\partial x} = 0; n_+(0,t) = 0; \frac{\partial n_+(L,t)}{\partial x} = 0; n_-(L,t) = 0
\end{aligned} \tag{5}$$

Note that the boundary conditions of charged species depend on whether the electrode is anode or cathode. At the high voltage electrode (x = 0), the number density of negatively charged species and the gradients of cations number density are zero when the electrode is a cathode (V < 0). Conversely, zero gradients of negative charged species and zero number density of positive ions are considered when the high voltage electrode is an anode (V > 0). For an AC electric field, the electrode changes periodically from a cathode to an anode, depending on the voltage sign of the high voltage electrode. For this reason, a cyclical variation of the previous boundary conditions at the high voltage electrode is imposed, consistent with a previous study [30].

The 1D system of equations was solved on desktop computers with basic first order time integration and spatial discretization. Consistent with Xiong et al. [37], the grid convergence was tested based on the Richardson extrapolation, and 200 grid points were selected with adequate accuracy.

Even with a simple 1D problem, an extensive parametric study is needed for the present unsteady problem. Therefore, unlike in Ref. [37], only one type of negatively charged molecule is described by Equation (2) and electrons are not separately considered. The behaviour of electrons may be deduced by that of negatively charged molecules in the limit of large mobility K_-. Similarly, the spatial asymmetry is of less significance, and only the centrally ionised layer ($H/L = 0.5$) is considered.

The key parameters of the present investigation are the amplitude and frequency of the voltage oscillations imposed at $x = 0$. The response of the different ions is characterised by mobility. To this end, the following results and discussion will be divided into two distinct cases: (a) the symmetric case in which both positive and negative ions have the same mobility, and (b) the asymmetric case with different mobilities of positive and negative ions. For all cases, $L = 1$ cm and $a = 1$ mm represent a typical flame thickness. The rate constants are selected as $k_i = 1 \times 10^{20}$ ions/m^3-s and $k_r = 2.4 \times 10^{-13}$ m^3/ions-s [23].

A system's dynamic response is closely tied to the various time scales that characterise the underlying physical and chemical processes. To support this observation, a parametric study is conducted, which shows how the trend of predicted current–voltage (I–V) behaviour is sensitive to a selected parameter.

In this present study, the current density describes a displacement current and a charge transport current.

It is calculated in the external circuit.

$$I = q_e K_+ n_+(L,t)E(L,t) - q_e K_- n_-(L,t)E(L,t) \tag{6}$$

The characteristic scales for number density, length, time, and voltage are defined as $n_0 = \sqrt{\frac{k_i}{k_r}}$ [37], $t_0 = T$, where $T = 1/f$ is the period of the imposed voltage oscillation, $L_0 = L$ and $V_0 = V_{\mathrm{RMS}}$. The relevant time scales are defined here. First, the time scales for the ionisation and recombination reactions are defined as:

$$\tau_i = \frac{n_0}{k_i} \tag{7}$$

$$\tau_r = \frac{1}{k_r n_0} \tag{8}$$

which implies that

$$\tau_i = \tau_r = \frac{1}{\sqrt{k_i k_r}} \tag{9}$$

Furthermore, the transport time scales for positive and negative ions are defined as:

$$\tau_{t_+} = \frac{L^2}{K_+ V_{\mathrm{RMS}}} \tag{10}$$

$$\tau_{t_-} = \frac{L^2}{K_- V_{\mathrm{RMS}}} \tag{11}$$

assuming that the ion transport is mainly by the mobility induced by the electric field. The non-dimensionalized variables are defined as:

$$\tilde{x} = \frac{x}{L_0}; \tilde{t} = \frac{t}{t_0}; \tilde{n} = \frac{n}{n_0}; \tilde{V} = \frac{V}{V_0} \tag{12}$$

Substituting the above non-dimensional variables into the dimensional governing equations, the non-dimensional forms for positive and negative ions and voltage are expressed as:

$$\frac{\partial \widetilde{n_+}}{\partial \tilde{t}} + \frac{\partial}{\partial \tilde{x}}\left[-\gamma_+^2 \frac{\partial \widetilde{n_+}}{\partial \tilde{x}} - \Omega_{t+}\widetilde{n_+}\frac{\partial \tilde{V}}{\partial \tilde{x}}\right] = \kappa^2[g - \widetilde{n_+}\widetilde{n_-}] \tag{13}$$

$$\frac{\partial \widetilde{n_-}}{\partial \tilde{t}} + \frac{\partial}{\partial \tilde{x}}\left[-\gamma_-^2 \frac{\partial \widetilde{n_-}}{\partial \tilde{x}} + \Omega_{t-}\widetilde{n_-}\frac{\partial \tilde{V}}{\partial \tilde{x}}\right] = \kappa^2[g - \widetilde{n_+}\widetilde{n_-}] \tag{14}$$

$$\frac{\partial^2 \tilde{V}}{\partial \tilde{x}^2} = -\frac{q_e L^2}{\varepsilon V_{\mathrm{RMS}}}(\widetilde{n_+} - \widetilde{n_-}) \tag{15}$$

where $\gamma_k^2 = D_k to/L_0^2$ (dimensionless diffusivity), $\Omega_{tk} = \frac{\tau_k}{T} = \frac{L^2}{K_k V_{\mathrm{RMS}} T}$ (dimensionless transport), and $\kappa^2 = n_0/k_i to$ (dimensionless ion rate coefficient), where $k = +, -$.

3. Results and discussion

As a first study to identify and formalise various characteristic time scales, the interpretation of physical observation, such as the flame response to frequency, is clearer and easy to understand by using the symmetric case first. The unsteadiness introduced a number of new parameters, hence it is not wise to complicate the result by starting the simulations with asymmetric conditions. The asymmetry case associated with the electron is viewed as a special case scenario of the general theory detailed in the second part of this section.

3.1. *Symmetric response*

As the baseline case study, $K_+ = K_- = 2.9 \times 10^{-4}$ m^2/s-V [38] is used such that the transport of the positive and negative ions are symmetric. Figure 2 shows a typical behaviour of variations in the current density over time for different frequencies of the voltage oscillation, for (a) $V_{\max} = 1$ kV and (b) $V_{\max} = 2$ kV. The saturation voltage V_{sat} in a DC configuration is 1.5 kV [37]. The time axis is normalised by the period $T = 1/f$. At each frequency, the response through one cycle of oscillation is shown after a limit cycle behaviour was achieved. Per sinusoidal voltage oscillation given in Equation (5), the dimensionless current $\tilde{I}$ flows from the electrode ($\tilde{x} = 0$) to the ground ($\tilde{x} = 1$) during the first half-period, i.e. the positive ions to the ground and negative ones to the electrode, and vice versa during the second half. The observed symmetry between the two half-periods is due to the identical values of the mobility of the positive and negative ions, $K_+ = K_-$. For $V_{\max} = 1$ kV (Figure 2(a)), the current response is close to sinusoidal, with an increased phase lag as the frequency is increased. Note that, as the frequency increases from 10 to 1000 Hz, the current density increases until it attenuates at 10,000 Hz. In contrast, for $V_{\max} = 2$ kV (Figure 2(b)) at $f = 10$ Hz, the quasi-steady flame response exhibits the saturation in the dimensionless current density at about 0.13 and an increased level of overshoot is seen at $f = 100$ Hz. At $f = 1000$ Hz, the initial rise in the current density is delayed first, followed by a more rapid rise to exceed the steady saturation condition by a significant amount. This behaviour is related to the overshoot seen for $f = 10$ Hz and $f = 100$ Hz and will be discussed in detail later. At a much higher frequency of $f = 10{,}000$ Hz, the current response is attenuated as in the $V_{\max} = 1$ kV case.

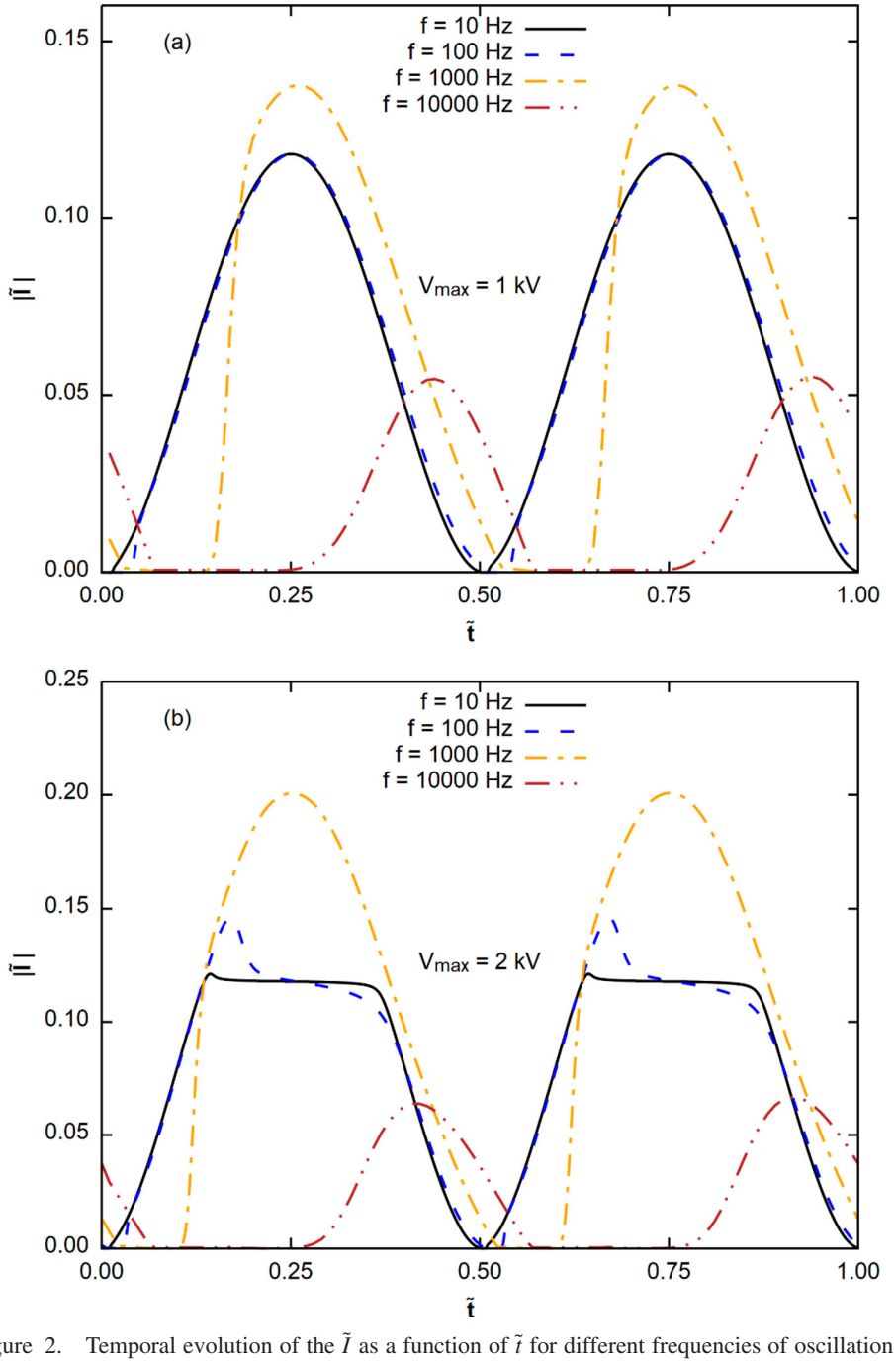

Figure 2. Temporal evolution of the $\tilde{I}$ as a function of $\tilde{t}$ for different frequencies of oscillation at $f = 10$, 100, 1000 and 10,000 Hz, for (a) $V_{\max} = 1$ kV and (b) $V_{\max} = 2$ kV.

Figure 3 shows the corresponding phase diagram of current density versus the voltage over the limit cycle, for (a) $V_{\max} = 1$ kV and (b) $V_{\max} = 2$ kV. The thick red curve shows

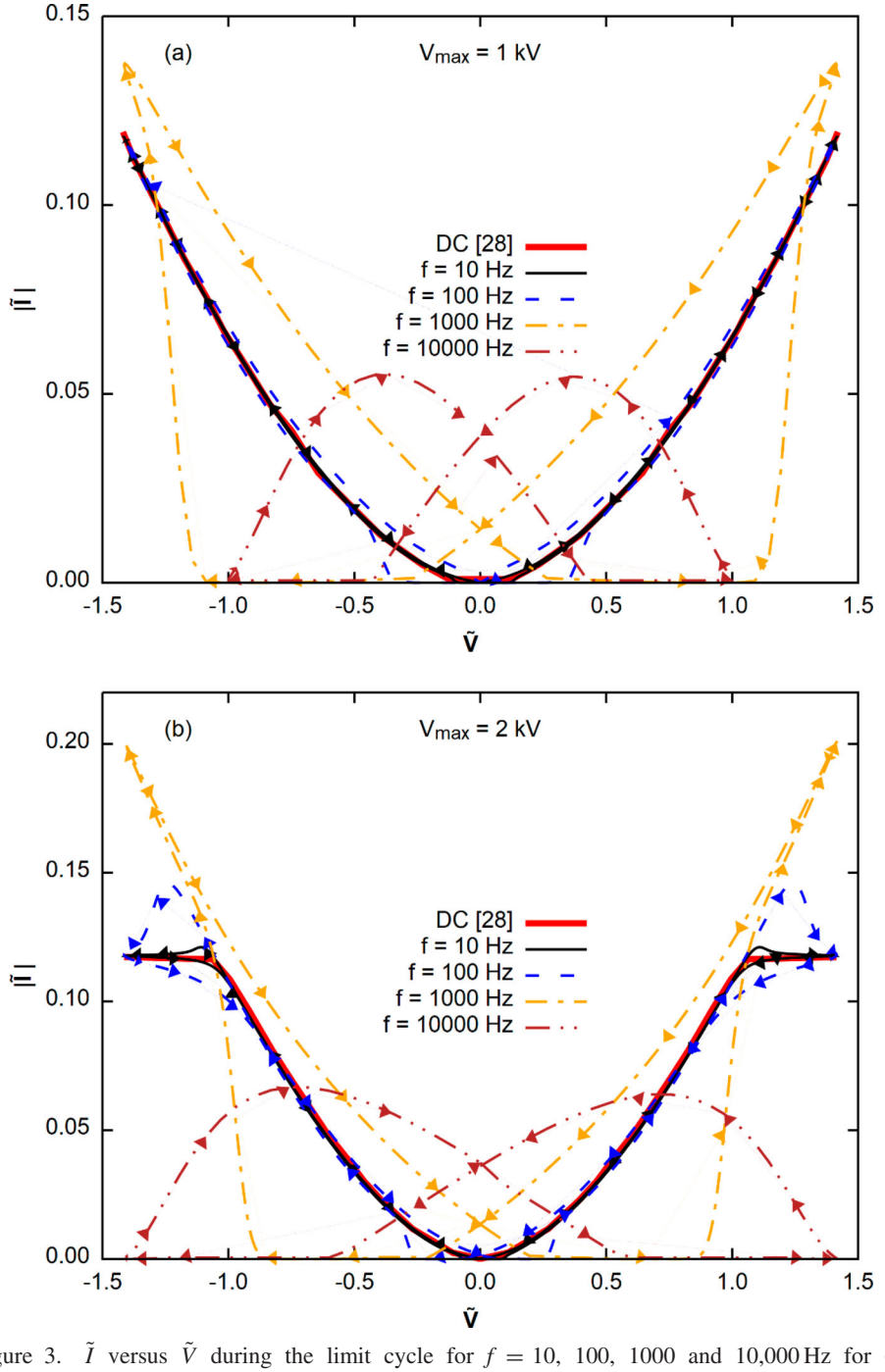

Figure 3. $\tilde{I}$ versus $\tilde{V}$ during the limit cycle for $f = 10$, 100, 1000 and 10,000 Hz for (a) $V_{\max} = 1$ kV and (b) $V_{\max} = 2$ kV.

the steady direct current (DC) result, i.e. the collection of steady solutions at the corresponding voltage at $x = 0$. The arrows on the unsteady response curves show the temporal progression over the cycle. At $f = 10$ Hz, for both voltages, the unsteady solution nearly follows the DC curve, except for the small overshoot shown at the onset of the steady solution for $V_{\max} = 2$ kV in Figure 3(b). As the frequency further increases to 1000 Hz, initially, the current rise lags significantly, but then rapidly rises to reach the dimensionless current density at 0.2, much higher than the DC saturation condition at 0.13. Finally, at a much higher frequency of $f = 10{,}000$ Hz, the response is largely attenuated with a long phase lag.

To explain why the current density increases with frequency from 10 to 1000 Hz and then decreases at 10,000 Hz, Figure 4 shows the spatial distribution of positive ions, $\widetilde{n_+}$, at different instants, $\tilde{t} = 0.1$, 0.15, 0.2, and 0.25, at frequencies of (a) 10, (b) 1000 and (c) 10,000 Hz for $V_{\max} = 2$ kV. The behaviour of the negative ions is symmetric for the same mobility. For $f = 10$ Hz at near quasi-steady condition, as the applied voltage ramps up over time, the ions are taken out of the reaction zone so that the ion concentration immediately drops down. At the same time, a significant increase in the ion concentration is seen at the boundary at $\tilde{x} = 1$. The peak ion concentration decreases slowly beyond $\tilde{t} = 0.15$ as the saturation condition is reached. This behaviour is consistent with the flame response to the DC voltage [39–42]. For higher frequency at $f = 1000$ Hz, however, the peak in the ion concentration does not decrease as much over time, dropping only by about 40% when the instantaneous voltage is at maximum at $\tilde{t} = 0.25$. This is attributed to the time lag in the response of the ion chemistry, which has the characteristic time of $\tau_i = 0.2$ ms, resulting effectively in a shielding action for ions. In fact, for $f = 1000$ Hz, at $\tilde{t} = 0.15$, the ions are still present in the flame zone even if the saturation condition is reached ($V(\tilde{t} = 0.15) = 1.62\,\text{kV} > V_{\text{sat}} = 1.5\,\text{kV}$ [37]). This behaviour is characterised by the ratio defined as:

$$\Omega_i = \frac{\tau_i}{t_{\text{sat}}} = \frac{1}{t_{\text{sat}}\sqrt{k_i k_r}} \tag{16}$$

where

$$t_{\text{sat}} = \sin^{-1}\left(\frac{V_{\text{sat}}}{V_{\max}}\right)\left(\frac{T}{2\pi}\right)$$

is the time at which the voltage reaches the DC saturation condition. For the conditions under study, $\Omega_i = 1$ is reached approximatively at $f = 700$ Hz, beyond which the ions remain in the reaction zone even if the saturation condition is reached.

Finally, for $f = 10{,}000$ Hz, the unsteady frequency is so high that, while the peak ion concentration is reduced and the overall ion layer is broadened, the ion concentration is still very low at the boundary. This implies that the frequency in the voltage oscillation is too high, such that the unsteady time scale is even shorter than that of the ion transport to produce a significant level of current flow at either side of the electrodes. The ratio of the transport time scale to the period of voltage oscillation is quantified as Ω_t (dimensionless transport in Section 2). For the conditions under study, $\Omega_t = 1$ is reached approximately at $f = 4000$ Hz. Therefore, the ions hardly reach the electrode boundary at $f = 10{,}000$ Hz, leading to a significantly reduced current density.

The resultant effect is clearly seen in Figure 5, where the spatial voltage distributions for $\tilde{t} = 0.1$, 0.15 and 0.25 are shown. At $f = 1000$ Hz, the shielding of ions yields a voltage

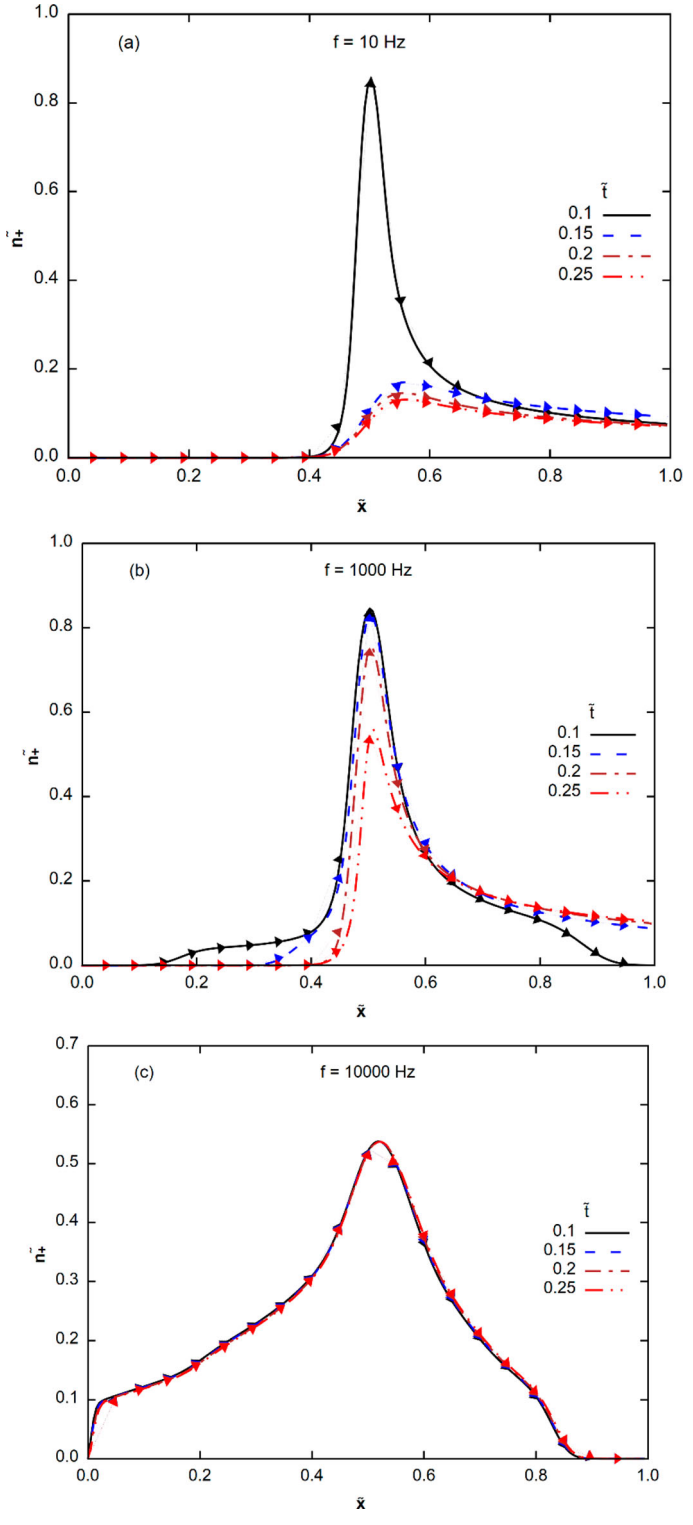

Figure 4. Distribution of $\widetilde{n_+}$ in function of $\tilde{x}$ at (a) $f = 10\,\text{Hz}$, (b) $f = 1000\,\text{Hz}$ and (c) $f = 10{,}000$ï£¡ï£¡Hz for $\tilde{t} = 0.1, 0.15, 0.2$ and 0.25 at $V_{\max} = 2\,\text{kV}$.

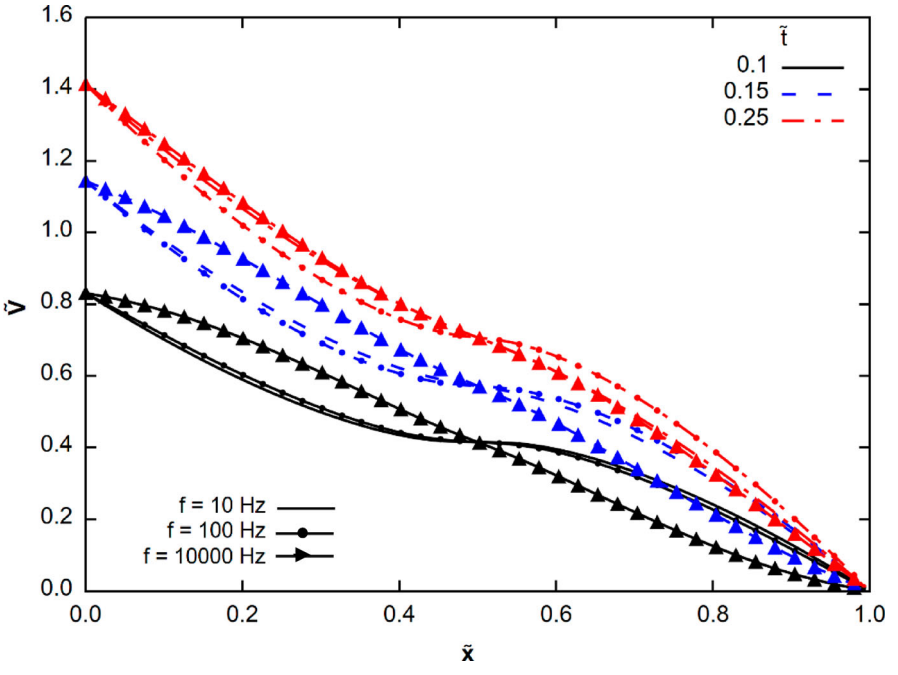

Figure 5. Distribution of $\tilde{V}$ in function of x at $f = 10$, 1000 and 10,000 Hz for $\tilde{t} = 0.1$, 0.15, 0.2 and 0.25 at $V_{\max} = 2$ kV.

plateau region and a larger voltage gradient outside the shield region. Since the current density is proportional to the electric field, $\tilde{E} = d\tilde{V}/d\tilde{x}$, this results in a current density higher than the maximum DC saturation value as shown in Figures 2 and 3. At $f = 10{,}000$ Hz, while the electric field strength is comparable, there is little ion transport at the electrode, resulting in a much lower current density. The shielding effect as seen in Figure 5 is also present in the DC configuration, as reported in Ref. [43]. In the sub-saturated regime, a large amount of charged species are 'trapped' in the flame zone, with the remaining charges redistributed to minimise their potential. In the saturated regime, however, all generated ions totally migrate to the electrodes and no further charges remain in the flame zone. Therefore, such 'effective shielding' behaviour at higher voltages beyond saturated conditions is a unique feature of the unsteady flame dynamics at high frequencies and explains the overshoot in the current response shown in Figure 3.

In summary, the dynamical response of the ion layers subjected to an AC electric field varies significantly depending on the characteristic time scales associated with the imposed oscillation, ion chemistry, and transport processes, resulting in the net I–V response that is drastically different from what could be expected from the DC configuration.

For practical implication in terms of the I–V characteristics, the ion layer response to an AC electric field is measured by the root mean square (RMS) current density as a function of the frequency. Figure 6 shows the RMS current density normalised by the RMS current density for the quasi-steady ($f \to 0$) limit at the corresponding voltage. The non-monotonic current response to the frequency is clearly seen in both cases of $V_{\max}$; as the frequency increases, the current increases above the DC saturation value as the $\Omega_i = 1$ condition is reached, and then falls off as the frequency exceeds the $\Omega_t = 1$ condition. The

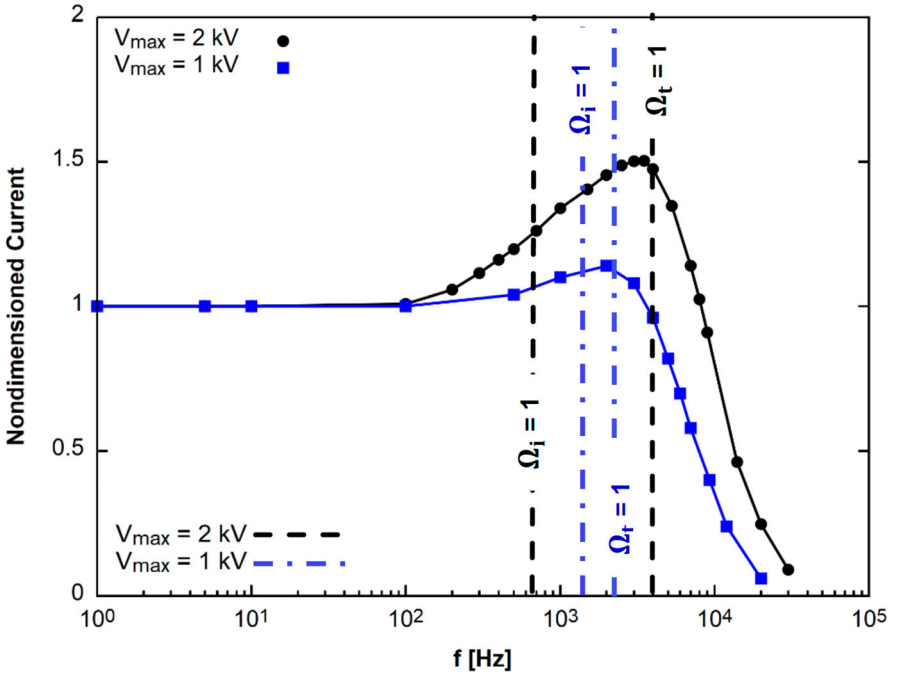

Figure 6. The non-dimensional current in function of f at $V_{\max} = 1$ and 2 kV.

Table 1. Four cases of k_i under study.

k_i (ions/m^3-s)	τ_i (ms)	$f_{\Omega_i=1}$ (Hz)	$f_{\Omega_t=1}$ (Hz)
1×10^{19}	0.65	~ 55	~ 4000
1×10^{20}	0.2	~ 700	~ 4000
1×10^{22}	2×10^{-2}	~ 8000	~ 4000
1×10^{25}	6.5×10^{-4}	$\sim 40{,}000$	~ 4000

frequency range between Ω_i and Ω_t narrows down as $V_{\max}$ becomes lower, such that the nonmonotonic rise behaviour is expected to vanish as the $\Omega_i = 1$ and $\Omega_t = 1$ conditions coincide.

Figure 6 demonstrates that the I–V characteristics of the flames subjected to an AC voltage may vary depending on the relative magnitude between the chemical (ionisation/recombination) and transport time scales. This behaviour is further explored in the following parametric studies. First, distinct ionisation versus recombination time scales are examined by considering four different values of k_i while fixing k_r at 2.4×10^{-13} m^3/ions-s. These are shown in Table 1. Figure 7 shows the corresponding non-dimensional RMS current as a function of f. As the ionisation time scale (τ_i) is reduced, the shielding effect is suppressed as the ionisation reactions can respond to the rapid voltage rise, resulting in a reduced current overshoot and nearly a monotonic decay is observed for $\tau_i = 6.5 \times 10^{-4}$ ms. Since the transport time scale is fixed in this parametric study, for all cases the peak in the current is reached at $f_{\Omega_t=1} = 4000$ Hz and decays nearly at the same rate.

Figure 8 illustrates the unsteady I–V response for the two extreme cases. For the rapid ionisation (a) $\tau_i = 6.5 \times 10^{-4}$ ms, the saturation condition is not reached even up to

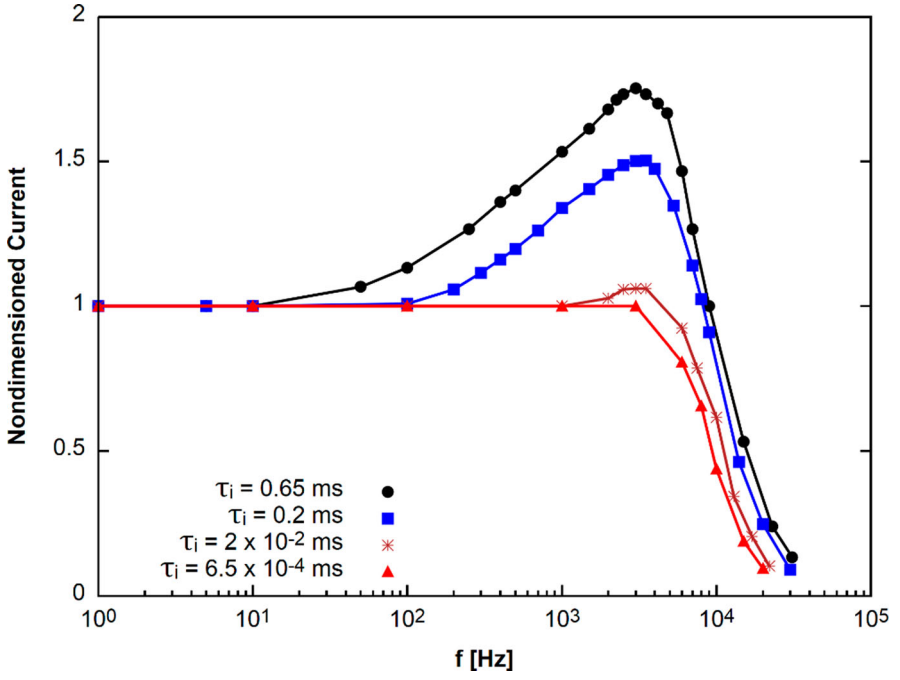

Figure 7. The non-dimensional current as a function of f for $\tau_i = 0.65$, 0.2, 2×10^{-2} and 6.5×10^{-4} ms at $V_{\max} = 2$ kV.

2 kV, and since the transport-limited attenuation is only reached at $f = 4000$ Hz, the three unsteady oscillation cases of $f = 10$–1000 Hz all nearly collapse on the DC response. On the other hand, for the slow ionisation (b) $\tau_i = 0.65$ ms, the saturation condition is reached at a much lower voltage at $V_{\text{sat}} \approx 450$ V, and the unsteady overshoot in the current is seen at a frequency as low as $f = 10$ Hz and continues to rise as the frequency is increased.

Figure 9 further highlights the contrasting behaviour of the response of the spatial ion distributions for (a) the fast ionisation ($\tau_i = 6.5 \times 10^{-4}$ ms) and (b) the slow ionisation ($\tau_i = 0.65$ ms) cases. At the same frequency of 1000 Hz, the fast ionisation reaction case (a) shows a nearly invariant spatial distribution of positive ions while the voltage was ramped up. On the other hand, for the slow ionisation case (b), the ion layers lag significantly as the voltage is ramped up, such that the level of ion concentration at the electrode boundary changes significantly, leading to the current density overshoot as seen in Figure 8.

To assess the effect of the ion transport time scale, three test cases are selected as shown in Table 2, where the transport time scale is varied by changing the distance between the electrodes, $L = 1$, 2 and 4 cm. Other parameters are fixed at $K_+ = 2.9 \times 10^{-4}$ m^2/s-V and $V_{\text{RMS}} = 1414$ V, and the ionisation and recombination time scales are also fixed to 0.2 ms. Figure 10 shows the expected behaviour: first, the peak current decreases as the transport time scale increases, because the ion transport cannot fully respond to the applied voltages at higher frequencies. Consequently, at higher oscillation frequencies the saturation condition is reached at the peak voltage significantly higher than V_{sat} at the corresponding DC condition. At $\tau_t = 4$ ms, ion transport becomes so slow that $f_{\Omega_i=1} > f_{\Omega_t=1}$, making the nonmonotonic increase in the current nearly nonexistent. The final decay in the current response is still dictated by the transport process, so that unlike in Figure 7, the 'cutoff'

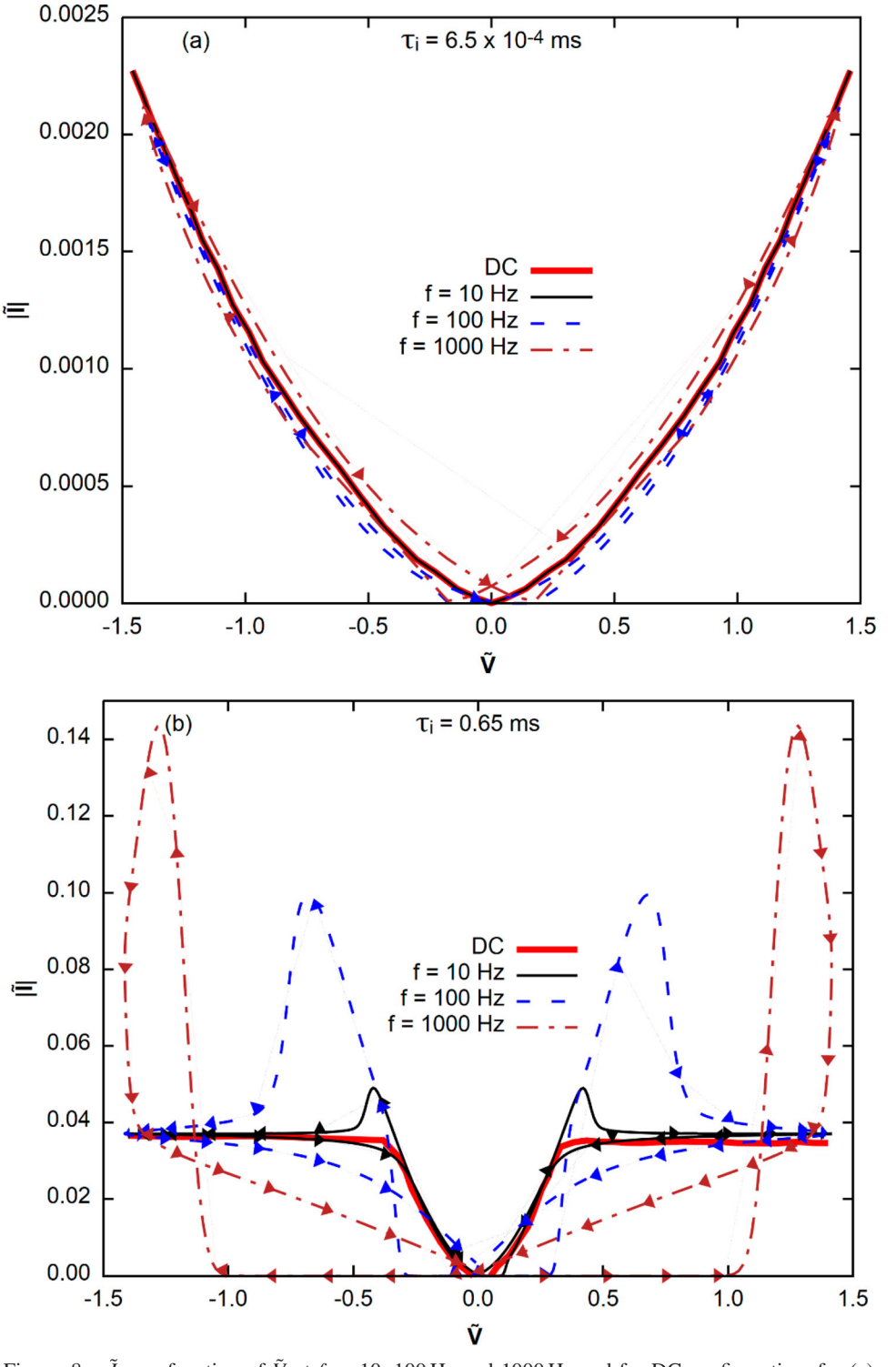

Figure 8. $\tilde{I}$ as a function of $\tilde{V}$ at $f = 10$, 100 Hz and 1000 Hz and for DC configuration, for (a) $\tau_i = 6.5 \times 10^{-4}$ ms and (b) $\tau_i = 0.65$ ms.

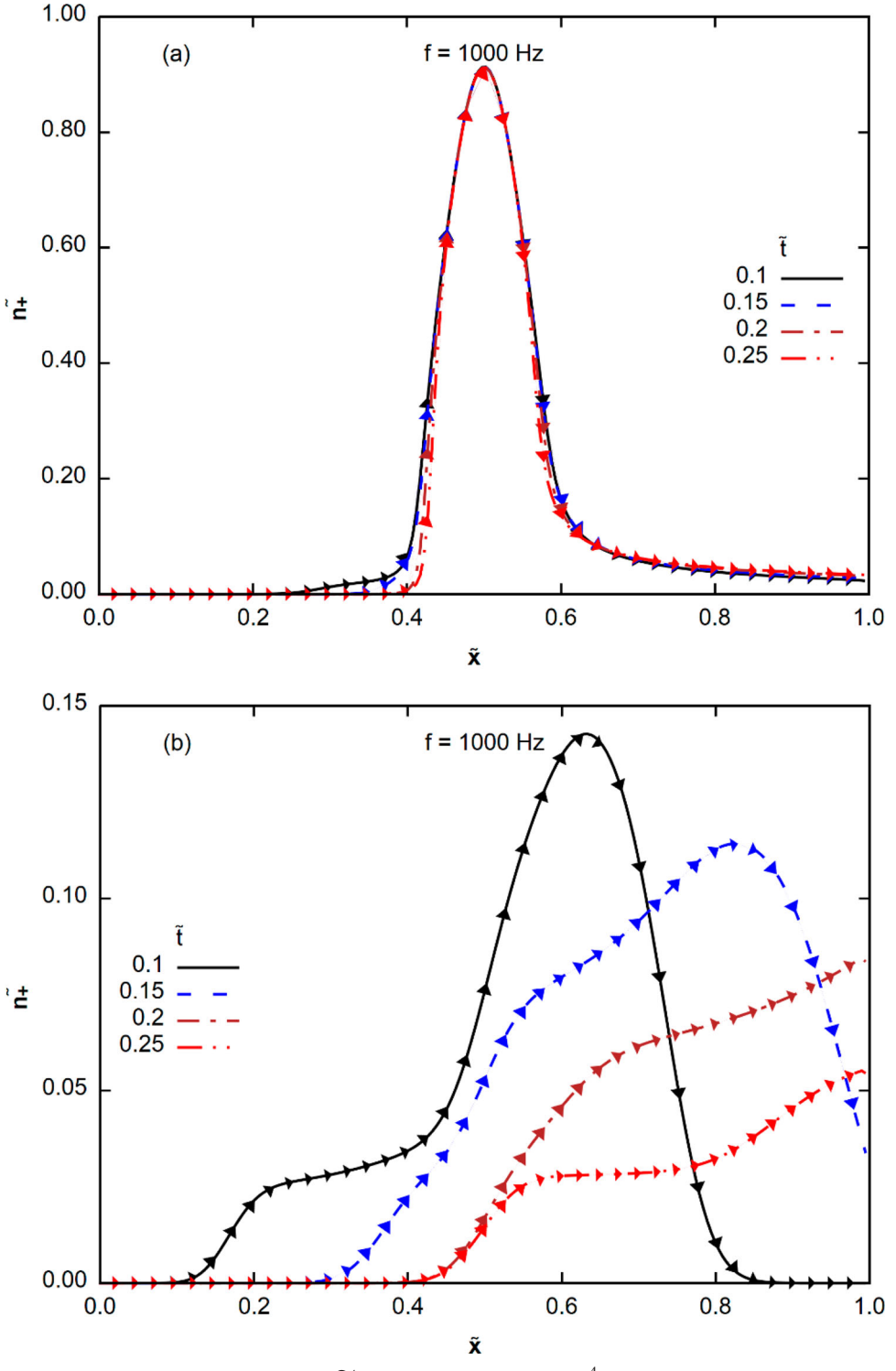

Figure 9. Spatial distribution of $\widetilde{n_+}$ for (a) $\tau_i = 6.5 \times 10^{-4}$ ms and (b) $\tau_i = 0.65$ ms, at $f = 1000$ Hz for $\tilde{t} = 0.1, 0.15, 0.2$ and 0.25.

Table 2. Test cases for different transport time scales.

L (cm)	τ_t (ms)	$f_{\Omega_i=1}$ (Hz)	$f_{\Omega_t=1}$ (Hz)
1	0.24	~ 700	~ 4000
2	0.97	~ 900	~ 1000
4	4	~ 1250	~ 250

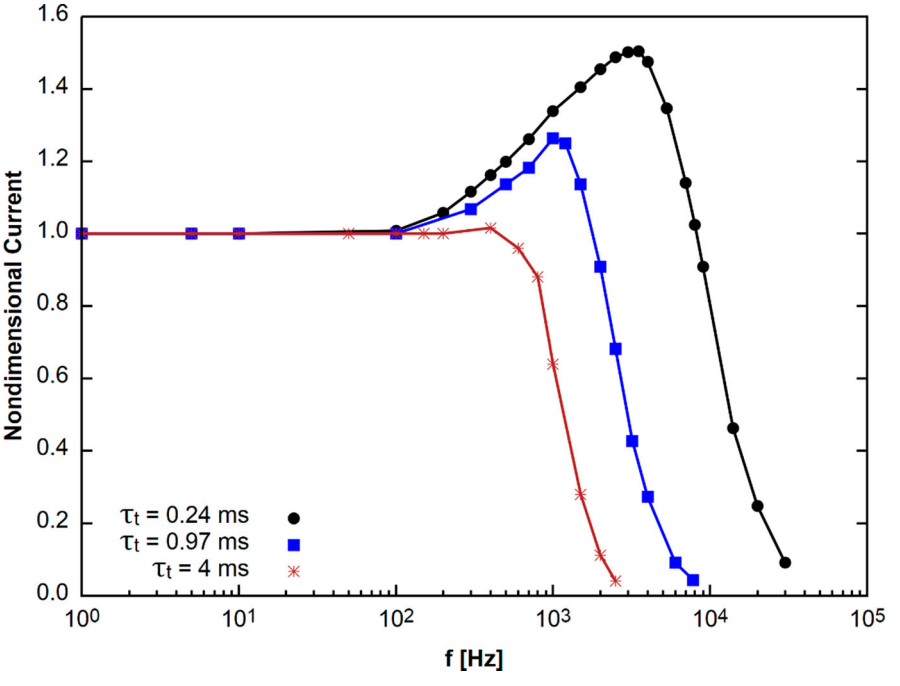

Figure 10. The non-dimensional current as a function of f for $\tau_t = 0.24$, 0.97 and 4 ms at $V_{\max} = 2$ kV.

frequency for the flame's low-pass filter behaviour is shifted as the transport time scale is increased.

Finally, the above studies so far considered symmetry in mobility, that is $K_+ = K_-$. In realistic flames, electrons are usually the dominant negative charges and thus a large asymmetry is expected in the mobility of the positive and negative ions. To represent such flame conditions, the following parametric study considers the ratio of the mobility of the negative to positive ions, $\sigma = K_-/K_+$, at 1, 10, and 1000, while K_+ is fixed at 2.9×10^{-4} m^2/s-V, as shown in Table 3.

Figure 11 shows the temporal evolution of the current density as a function of time for different $\sigma = 1$, 10, and 1000 at $f = 1000$ Hz. It shows an asymmetry of the electric current during the two half-periods. This is due to the difference in the mobility between negatively and positively charged species. The electric current in the first half-period corresponds to the amount of positive ions reaching the ground electrode. However, the electric current in the second half-period represents the amount of negative ions arriving at the

Table 3. Test cases for different σ.

σ	$f_{\Omega_i=1}$ (Hz)	$f_{\Omega_t=1}$ (Hz)	$f_{\Omega_{i^+}=1}$ (Hz)	$f_{\Omega_{i^-}=1}$ (Hz)
1	$\sim$700	$\sim$4000	$\sim$4000	$\sim$4000
10	$\sim$425	$\sim$22,000	$\sim$4000	$\sim$40,000
1000	$\sim$325	$\sim$30,000	$\sim$4000	$\sim$4,000,000

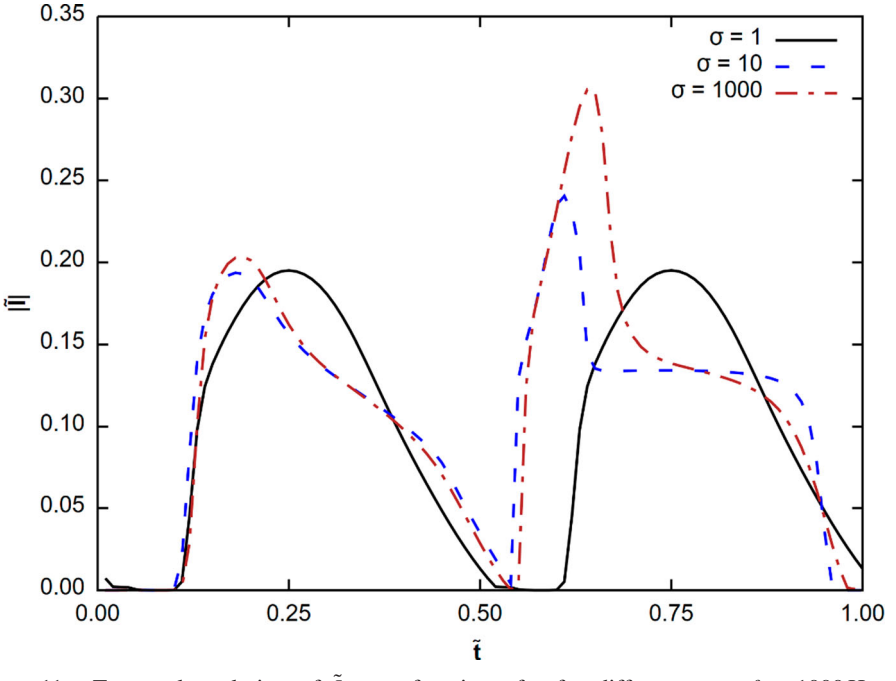

Figure 11. Temporal evolution of $\tilde{I}$ as a function of t for different σ at $f = 1000$ Hz, for $V_{\max} = 2$ kV.

ground electrode. For the three ratios 1, 10 and 1000, the electric current in the first half-period behaves in the similar way. This is explained by the fact that the first period is controlled by the positive ions whose mobility was fixed to $K_+ = 2.9 \times 10^{-4}$ m^2/s-V. On the other hand, the behaviour of the electric current density in the second half-period changes in proportion to the ratio. This parameter plays on the intensity of the peak which is increasing with σ because of the decrease in the transport time scale due to the high mobility of negatively charged species.

Figure 12 shows the non-dimensional current density as a function of frequency. As σ increases, the increased mobility of the negative ions enhances the current overshoot as well as the $f_{\Omega_i=1}$. Note that for the asymmetric mobilities between the positive and negative ions, the nonmonotonic overshoot behaviour is governed by the faster ions; for $\sigma = 1000$ which may represent a condition where electrons are the dominant negatively charged species, the maximum current is much more increased and occurs at a higher frequency. On the other hand, Table 3 shows that the resultant frequency $f_{\Omega_t=1}$ is closer to $f_{\Omega_{i^+}=1}$ than to $f_{\Omega_{i^-}=1}$, which implies that the slower process determines the unsteady attenuation behaviour. When the amount of ions with the lower mobility becomes attenuated near the

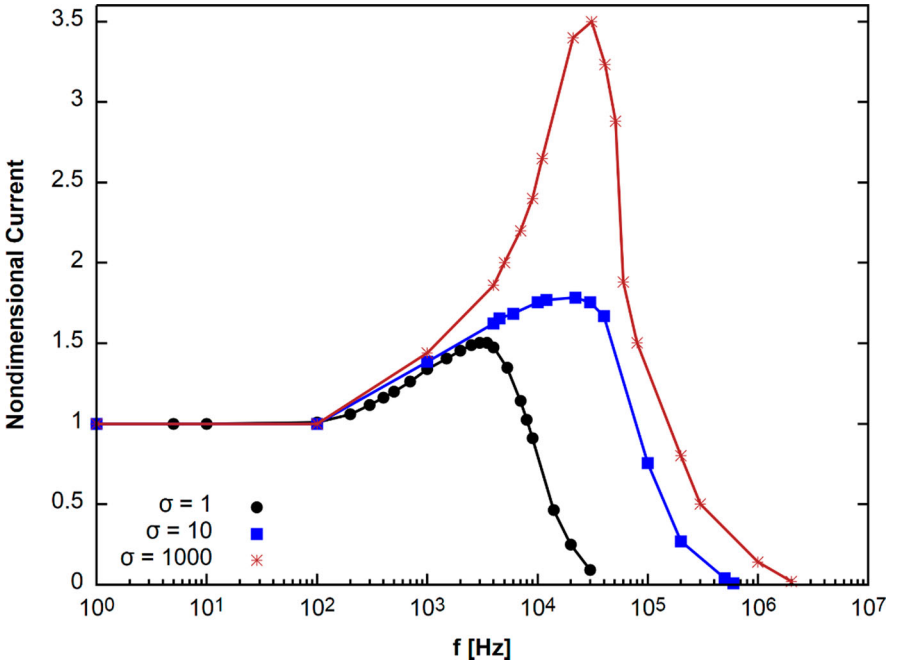

Figure 12. The non-dimensional current as a function of f for $\sigma = 1$, 10 and 1000 at $V_{\max} = 2\,\text{kV}$.

electrode, the amount of the charged species with the highest mobility is also instantly impacted because of the conservation of the current density. Furthermore, in contrast to the symmetric condition shown in Figure 10, the final current decay behaviour is a net result of the competing effect between the transport of positive and negative ions, hence the slope of the decay varies as the frequency is increased. The results shown in Figure 11 imply that the effects of AC electric fields on the real flames where large differences in the mobility of electrons and positive ions may lead to a complex I–V response that cannot be predicted from a simple quasi-steady extension of the flame response to DC electric fields.

To assess the effect of the ionisation and recombination time scale for the asymmetric case, four different values of k_i were considered while fixing k_r at 2.4×10^{-13} m^3/ions-s at $\sigma = 1000$. The results are shown in Table 4. Figure 13 shows the non-dimensional current as a function of the frequency. As the ionisation time scale (τ_i) is reduced, the shielding effect of low and high mobility charges is suppressed as the ionisation reactions can respond to the rapid voltage rise, resulting in a reduced current overshoot and a monotonic decay observed for $\tau_i = 6.45 \times 10^{-5}$ ms. Since the transport time scale is fixed in this parametric study, for all cases the peak in the current is reached at $f_{\Omega_i=1} = 30{,}000$ Hz and decays with the same slope.

To examine the effect of the ion transport time scale for the asymmetric case, three test cases are selected as shown in Table 5, where the transport time scale is varied by changing the distance between the electrodes, $L = 1$, 4 and 8 cm. Other parameters are fixed at $\sigma = 1000$ and $V_{\text{RMS}} = 1.414$ kV, and the ionisation and recombination time scales are also fixed at 0.2 ms. Figure 14 shows the same behaviour described in the symmetric case. In fact, the peak current decreases as the transport time scale increases, Also, the

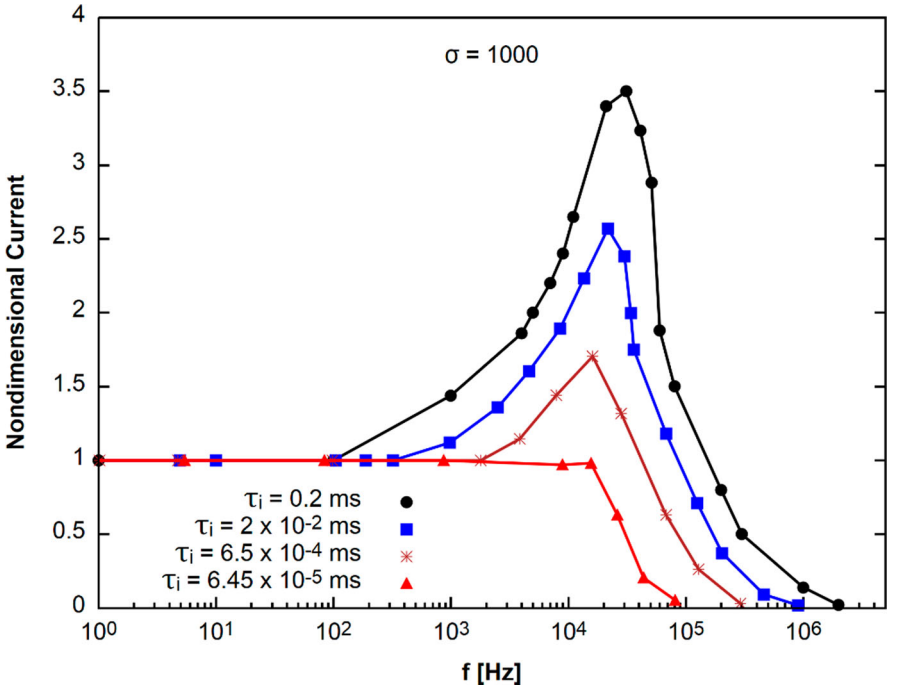

Figure 13. The non-dimensional current as a function of f for $\tau_i = 0.2$, 2×10^{-2}, 6.5×10^{-4} and 6.45×10^{-5} ms at $V_{\max} = 2$ kV for $\sigma = 1000$.

Table 4. Four cases of k_i under study, for the asymmetric case at $\sigma = 1000$.

k_i (ions/m^3-s)	τ_i (ms)	$f_{\Omega_i=1}$ (Hz)	$f_{\Omega_{i^+}=1}$ (Hz)	$f_{\Omega_{i^-}=1}$ (Hz)	$f_{\Omega_i=1}$ (Hz)
1×10^{20}	0.2	$\sim$325	$\sim$4000	$\sim$4,000,000	$\sim$30,000
1×10^{22}	2×10^{-2}	$\sim$2000	$\sim$4000	$\sim$4,000,000	$\sim$30,000
1×10^{25}	6.5×10^{-4}	$\sim$10,000	$\sim$4000	$\sim$4,000,000	$\sim$30,000
1×10^{27}	6.45×10^{-5}	$\sim$50,000	$\sim$4000	$\sim$4,000,000	$\sim$30,000

Table 5. Test cases for different transport time scales at $\sigma = 1000$.

L (cm)	τ_{i^+} (ms)	τ_{i^-} (ms)	$f_{\Omega_i=1}$ (Hz)	$f_{\Omega_{i^+}=1}$ (Hz)	$f_{\Omega_{i^-}=1}$ (Hz)	$f_{\Omega_i=1}$ (Hz)
1	0.24	0.24×10^{-3}	$\sim$325	$\sim$4000	$\sim$4,000,000	$\sim$30,000
4	4	4×10^{-3}	$\sim$800	$\sim$250	$\sim$250,000	$\sim$2000
8	15.2	15.2×10^{-3}	$\sim$1200	$\sim$60	$\sim$60,000	$\sim$500

'cutoff' frequency for the flame's low-pass filter behaviour is shifted as the transport time scale is increased.

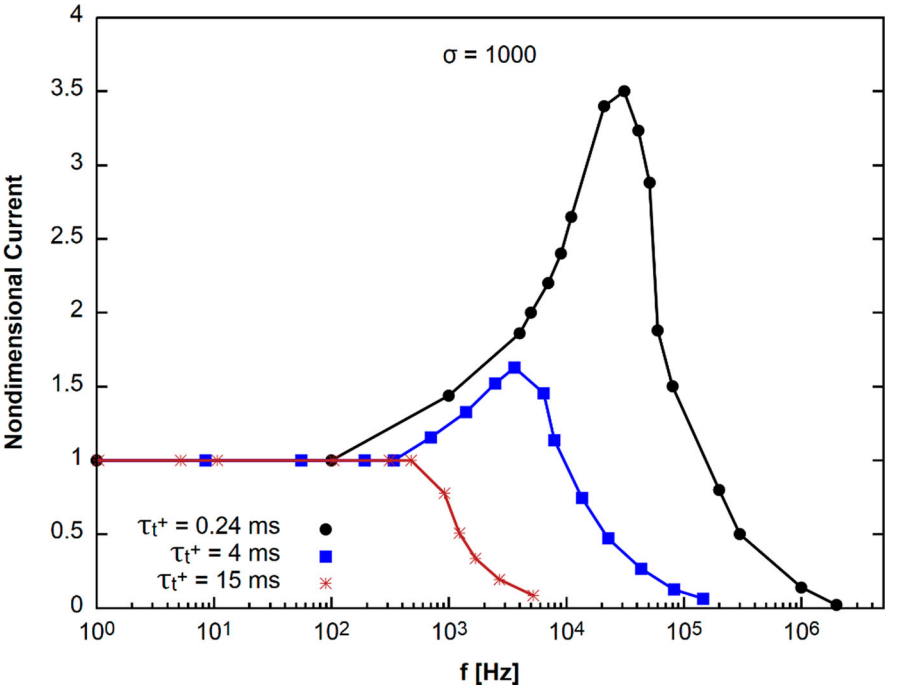

Figure 14. The non-dimensional current as a function of f for $\tau_{t^+} = 0.24$, 4 and 15 ms at $V_{\max} = 2$ kV for $\sigma = 1000$.

4. Conclusions

A simplified one-dimensional analysis was conducted for an ion layer representing a flame in response to AC voltage oscillations, as an attempt to provide insights into the fundamental characteristics of the flame response to unsteady sub-breakdown electric fields. While the present one-dimensional model is unable to predict the ionic wind effect, the systematic parametric study reveals the general flame behaviour in terms of different characteristic time scales associated with the ionisation and transport processes. The mathematical model was set up to represent all essential processes in a simplified manner: ionisation, recombination, and ion transport by electric mobility, while the molecular diffusion process for ions was included but was found to be unimportant.

The most important finding of the study is that the flame subjected to highly unsteady electric fields may exhibit saturation voltage and current that are significantly higher than those expected from the quasi-steady counterpart based on the DC analysis. A typical I–V response as the AC frequency is increased is the nonmonotonic current increase as the unsteady time scale becomes comparable to the ionisation time scale. The current reaches a peak as the unsteady time scale becomes comparable to the ion transport time scales determined by mobility. The unique unsteady behaviour is attributed to the produced ions *trapped* between the two electrodes, also known as the shielding effect, as the voltage changes too rapidly for the ions to reach the electrodes. As the frequency is further increased, the entire ion layer does not respond to the AC electric field at all, leading to the net zero current and ion transfer.

Further parametric studies revealed that the peak current, the frequencies at which the I–V curve rises and falls depend on the specific characteristic times for ionisation and mobility transport. For a case with strong asymmetry in the mobility of the positive and negative ions, the shielding effect is dominated by the ions with a higher mobility to yield a higher current overshoot, while the frequency at the current peak is governed by the characteristic transport time of ions with the slow mobility. The simplified analysis suggests that the response of real flames with complex chemistry to the AC electric field may be well predicted by a proper identification of key characteristic time scales for the dominant ion chemistry and transport.

Finally, the current overshoot behaviour observed in this study may suggest that the net effect of the electric field in the real multi-dimensional flames subjected to unsteady fluctuations may be more significant than could be expected from the quasi-steady flame analysis. Detailed multi-dimensional simulations are currently being investigated and the resulting ionic wind effects will be reported in future work.

Acknowledgements

The authors would like to thank Professor Min Suk Cha at KAUST for helpful comments during the technical analysis.

Disclosure statement

No potential conflict of interest was reported by the author(s).

Funding

The work was sponsored by the King Abdullah University of Science and Technology (KAUST).

ORCID

Hong G. Im http://orcid.org/0000-0001-7080-1266

References

[1] E. Place and F. Weinberg, *Electrical control of flame carbon*. Proc. Royal Soc. Lond. Ser. A Math. Phys. Sci. 289 (1966), pp. 192–205.
[2] D.R. Hardesty and F.J. Weinberg, *Electrical control of particulate pollutants from flames*. Symp. (Int.) Combust. 14 (1973), pp. 907–918.
[3] M. Saito, T. Arai and M. Arai, *Control of soot emitted from acetylene diffusion flames by applying an electric field*. Combust. Flame 119 (1999), pp. 356–366.
[4] M.S. Cha, S.M. Lee, K.T. Kim and S.H. Chung, *Soot suppression by nonthermal plasma in coflow jet diffusion flames using a dielectric barrier discharge*. Combust. Flame 141 (2005), pp. 438–447.
[5] D.G. Park, B.C. Choi, M.S. Cha and S.H. Chung, *Soot reduction under DC electric fields in counterflow non-premixed laminar ethylene flames*. Combust. Sci. Technol. 186 (2014), pp. 644–656.
[6] M.S. Cha and Y. Lee, *Premixed combustion under electric field in a constant volume chamber*. IEEE Trans. Plasma Sci. 40 (2012), pp. 3131–3138.
[7] E. Guenault and R. Wheeler, *The propagation of flame in electric fields. Part II. The effects of transverse fields*. J. Chem. Soc. (Resumed) 423 (1932), pp. 2788–2793.
[8] H.C. Jaggers and A. von Engel, *The effect of electric fields on the burning velocity of various flames*. Combust. Flame 16 (1971), pp. 275–285.

[9] R.J. Bowser and F.J. Weinberg, *The effect of direct electric fields on normal burning velocity*. Combust. Flame 18 (1972), pp. 296–300.
[10] S.H. Won, S.K. Ryu, M.K. Kim, M.S. Cha and S.H. Chung, *Effect of electric fields on the propagation speed of tribrachial flames in coflow jets*. Combust. Flame 152 (2008), pp. 496–506.
[11] R. Noorani and R. Holmes, *Effects of electric fields on the blowoff limits of a methane-air flame*. AIAA J. 23 (1985), pp. 1452–1454.
[12] M. Belhi, P. Domingo and P. Vervisch, *Direct numerical simulation of the effect of an electric field on flame stability*. Combust. Flame 157 (2010), pp. 2286–2297.
[13] M.K. Kim, S.K. Ryu, S.H. Won and S.H. Chung, *Electric fields effect on liftoff and blowoff of nonpremixed laminar jet flames in a coflow*. Combust. Flame 157 (2010), pp. 17–24.
[14] M.K. Kim, S.H. Chung and H.H. Kim, *Effect of AC electric fields on the stabilization of premixed bunsen flames*. Proc. Combust. Inst. 33 (2011), pp. 1137–1144.
[15] J. Lawton, P.J. Mayo and F.J. Weinberg, *Electrical control of gas flows in combustion processes*. Proc. Royal Soc. A303 (1968), pp. 275–298.
[16] J. Lawton and F.J. Weinberg, *Electrical Aspects of Combustion*, Clarendon Press, Oxford, 1969, pp. 336–340.
[17] F. Carleton and F. Weinberg, *Electric field-induced flame convection in the absence of gravity*. Nature 330 (1987), pp. 635–636.
[18] S. Marcum and B. Ganguly, *Electric-field-induced flame speed modification*. Combust. Flame 143 (2005), pp. 27–36.
[19] A.M. Drews, L. Cademartiri, M.L. Chemama, M.P. Brenner, G.M. Whitesides and K.J.M. Bishop, *AC electric fields drive steady flows in flames*. Phys. Rev. E 86 (2012), p. 036314.
[20] D.G. Park, S.H. Chung and M.S. Cha, *Bidirectional ionic wind in nonpremixed counterflow flames with DC electric fields*. Combust. Flame 168 (2016), pp. 138–146.
[21] J.M. Goodings, D.K. Bohme and C.-W. Ng, *Detailed ion chemistry in methane-oxygen flames. I. Positive ions*. Combust. Flame 36 (1979), pp. 27–43.
[22] J.M. Goodings, D.K. Bohme and C.-W. Ng, *Detailed ion chemistry in methane-oxygen flames. II. Negative ions*. Combust. Flame 36 (1979), pp. 45–62.
[23] A.B. Fialkov, *Investigations on ions in flames*. Prog. Energy Combust. Sci. 23 (1997), p. 399.
[24] J. Han, M. Belhi, F. Bisetti and S.M. Sarathy, *Numerical modeling of ion transport in flames*. Combust. Theory Model. 19(6) (2015), pp. 744–772.
[25] J. Han, M. Belhi, T. Casey, F. Bisetti, H. Im and J. Chen, *The curve characteristics of burner-stabilized premixed flames: Detailed and reduced models*. Proc. Combust. Inst 36(1) (2017), pp. 1241–1250.
[26] M. Belhi, B.J. Lee, F. Bisetti and H.G. Im, *A computational study of the effects of DC electric fields on non-premixed counterflow methane-air flames*. J. Phys. D: Appl. Phys. 50 (2017), p. 494005.
[27] F. Bisetti and M. El Morsli, *Calculation and analysis of the mobility and diffusion coefficient of thermal electrons in methane/air premixed flames*. Combust. Flame 159 (2012), pp. 3518–3521.
[28] F. Bisetti and M. El Morsli, *Kinetic parameters, collision rates, energy exchanges and transport coefficients of non-thermal electrons in premixed flames at sub-breakdown electric field strengths*. Combust. Theory Model. 18 (2014), pp. 148–184.
[29] M. Belhi, J. Han, T.A. Casey, J.Y. Chen, H.G. Im, S.M. Sarathy and F. Bisetti, *Analysis of the current-voltage curves and saturation currents in burner-stabilised premixed flames with detailed ion chemistry and transport models*. Combust. Theory Model. 22(5) (2018), pp. 939–972.
[30] M. Belhi, P. Domingo and P. Vervisch, *Modeling of the effect of DC and AC electric fields on the stability of a lifted diffusion methane/air flame*. Combust. Theory Model. 17(4) (2013), pp. 749–787.
[31] S.M. Lee, C.S. Park, M.S. Cha and S.H. Chung, *Effect of electric fields on the liftoff of nonpremixed turbulent jet flames*. IEEE Trans. Plasma Sci. (2005), pp. 1703–1709.
[32] S.H. Won, S.K. Ryu, M.K. Kim, M.S. Cha and S.H. Chung, *Effect of electric fields on the propagation speed of tribrachial flames in coflow jets*. Combust. Flame (2008), pp. 496–506.
[33] C.S. MacLatchy, R.M. Clements and P.R. Smy, *An experimental investigation of the effect of microwave radiation on a propane-air flame*. Combust. Flame 45 (1982), pp. 161–169.

[34] D.G. Park, S.H. Chung and M.S. Cha, *Dynamic responses of counterflow nonpremixed flames to AC electric field*. Combust. Flame 198 (2018), pp. 240–248.
[35] C. Guerra-Garcia and M. Martinez-Sanchez, *Counterflow nonpremixed flame DC displacement under AC electric field*. Combust. Flame 162 (2015), pp. 4254–4263.
[36] L. Esclapez, V. Ricchiuti, J.B. Bell and M.S. Day, *A spectral deferred correction strategy for low Mach number reacting flows subject to electric fields*. Combust. Theory Model. 24(2) (2020), pp. 194–220.
[37] Y. Xiong, D.G. Park, B.J. Lee, S.H. Chung and M.S. Cha, *DC field response of onedimensional flames using an ionized layer model*. Combust. Flame (2016), pp. 3513–3520.
[38] M.J. Papac, *Electrical Aspects of Gaseous Fuel Flames for Microgravity Combustion and Combustion Control*, University of California, Irvine, 2005.
[39] S. Karnani and D.R. Rankin, *Detailed characterization of DC electric field effects on small non-premixed flames*. Combust. Flame 162 (2015), pp. 2865–2872.
[40] A. Sakhrieh, G. Lins, F. Dinkelacker, T. Hammer, A. Leipertz and D.W. Branston, *The influence of pressure on the control of premixed turbulent flames using an electric field*. Combust. Flame 143 (2005), pp. 313–322.
[41] F. Borgatelli and D. Dunn-Rankin, *Behavior of a small diffusion flame as an electrically active component in a high-voltage circuit*. Combust. Flame 159 (2012), pp. 210–220.
[42] K. Yamashita, S. Karnani and D. Dunn-Rankin, *Numerical prediction of ion current from a small methane jet flame*. Combust. Flame 156 (2009), pp. 1227–1233.
[43] M.D. Renzo, J. Urzay, P.D. Palma, M.D. de Tullio and G. Pascazio, *The effects of incident electric fields on counterflow diffusion flames*. Combust. Flame 193 (2018), pp. 177–191.